Open Ceramics 16 (2023) 100474

Contents lists available at ScienceDirect

Open Ceramics

journal homepage: www.sciencedirect.com/journal/open-ceramics

Masked stereolithography of wollastonite-diopside glass-ceramics from novel silicone-based liquid feedstock

Hamada Elsayed [a,b,*], Franco Matías Stabile [c,d], Gianpaolo Savio [e], Enrico Bernardo [a,**]

[a] Department of Industrial Engineering, Università degli Studi di Padova, Padova, Italy
[b] Refractories, Ceramics and Building Materials Department, National Research Centre, Cairo, 12622, Egypt
[c] Technology Center of Mineral Resources and Ceramic (CETMIC), CIC-CONICET-UNLP, Manuel B. Gonnet, Argentina
[d] Department of Chemical Engineering, Universidad Nacional de La Plata, La Plata, Argentina
[e] Department of Civil, Environmental and Architectural Engineering: Dept. ICEA, University of Padova, Padova, Italy

ARTICLE INFO

Handling Editor: Dr P Colombo

Keywords:
Stereolithography
Preceramic polymers
Wollastonite-diopside
Emulsion
Liquid feedstock

ABSTRACT

Silicate bioceramics, including systems based on the simultaneous presence of wollastonite ($CaSiO_3$) and diopside ($CaMgSi_2O_6$), are of great interest in bone tissue engineering applications, especially in form of variously shaped three-dimensional scaffolds, as determined by application of several additive manufacturing technologies. In this framework, silicone resins, properly modified with CaO- and MgO-based fillers and blended with photocurable acrylates, are attractive both as precursors and as feedstock for additive manufacturing technologies, including stereolithography. The use of powder fillers, however, may lead to issues with homogeneity or with printing resolution (owing to light scattering). The present paper aims at presenting the first results from a new concept of incorporation of CaO and MgO, relying on salts dispersed in emulsion within a photocurable silicone/acrylate blend. Direct firing at 1100 °C of printed scaffolds successfully produced wollastonite-diopside glass-ceramic scaffolds, with a very fine crystal distribution. The strength-to-density was tuned by operating either on the topology of scaffolds or on the firing atmosphere (passing from air to N_2).

1. Introduction

The potential of additive manufacturing (also known as '3D printing') technologies has revolutionized the shaping of components in many material domains, such as metals, polymers, ceramics and composites [1]. A key to success is the controlled placement of material 'where it is desired' and/or 'where it is needed'. In the first case, as an example, additive manufacturing easily offers dense components with multimaterial assembly, which in turn leads to controlled gradients of functionality [2]. In the second case, additive manufacturing has the undoubted advantage of developing cellular materials even with particularly complex topology, in turn enabling a fine-tuning of the property/porosity correlations, typically expressed by enhanced stiffness/mass and strength/mass ratios [3].

Topological optimization is particularly appreciated in the field of biomaterials [4]; in the subfield of bioceramics, this is of fundamental interest for highly porous scaffolds, to be used for bone tissue repair or integration [5]. The application of complex topologies, however, implies significant challenges, from the computation of the geometrical model (to be implemented in the 3D-printer) to the quite complex compatibility achievement between feedstock and adopted technology. The latter point is very delicate, since inadequate processing conditions may easily degrade the geometrical correlation between model and final product, especially for nominally refined stereolithography-based technologies [6]. Beyond shrinkage, printed ceramic scaffolds may exhibit thicker struts (and lower overall porosity), compared to the model, simply as a consequence of light scattering from solid powders suspended in photocurable resin (curing may occur outside the theoretical projection area - defined by horizontal cross-sections of the models – with an extension of solid occupancy in each printed layer [6,7]).

A solution to scattering is offered by liquid precursors for ceramics, based on preceramic polymers [8]. This particular class of polymers, typically based on Si atoms bridged by O, N or C atoms, has always attracted interest for the possibility to shape a component in the polymer state, coupled with transformation into a ceramic, by thermal treatment

* Corresponding author. Department of Industrial Engineering, Università degli Studi di Padova, Padova, Italy.
** Corresponding author.
E-mail addresses: hamada.elsayed@unipd.it (H. Elsayed), enrico.bernardo@unipd.it (E. Bernardo).

https://doi.org/10.1016/j.oceram.2023.100474
Received 7 February 2023; Received in revised form 13 September 2023; Accepted 22 September 2023
Available online 22 September 2023

above 500 °C [9]. A key progress, in recent years, concerns the application of stereolithography as the adopted polymer-shaping technology, realized through engineering of precursors, at different levels. On the one hand, photocurable silicones are already available on the market [8], on the other non-photosensitive silicones may be used by 'grafting' of photocurable moieties [10] or, more immediately, by direct blending with acrylates [7,11].

Silicones, as a fundamental part of preceramic polymers, can be engineered also in the perspective of final application. Oxide inclusions, mostly in the form of carbonate and hydroxide powders, dispersed in the polymer matrix, are known to yield a vast range of silicate bioceramics [7,12–16]. The high reactivity of the silica-based residue, resulting from the thermal decomposition of silicones, with nano- and micro-sized oxide inclusions, generally favors low processing temperatures and high phase purity [7]. Especially operating with alkali borates and phosphates, silicate synthesis is further enhanced by the formation of liquid phase (catalyzing ionic diffusion), remaining as intergranular glass phase after cooling. The products may be classified as glass-ceramics ('polymer-derived glass-ceramics') according to the nearly perfect match in the final phase assemblage between polymer-derived materials and glass-ceramics from the thermal treatment of parent glasses with the same overall oxide composition [7,14]. The fillers, being proposed in form of powders, obviously lead to the above-mentioned issue of light scattering and coarsening of printed structures [7].

This paper presents an original approach to 'polymer-derived glass-ceramics' based on wollastonite-diopside coupling - a highly appreciated bioceramic system [11,17,18] -, relying on blends of enhanced homogeneity. Calcium and magnesium salts are not considered as solid powders but dispersed as liquid droplets. These droplets are homogeneously distributed, by emulsification, in a particular matrix resulting from the mixing of a commercial non-photocurable silicone with a commercial photocurable acrylate resin. The dispersion of droplets followed experiences concerning water-in-oil emulsions [19]. A correct selection of surfactant formulation and content is known to yield highly dispersed liquid nanodroplets [20,21].

Although printing was performed by means of a low resolution apparatus, based on masked stereolithography, the emulsion approach effectively led to nearly transparent and highly homogeneous scaffolds, even in the presence of multiple salts (besides CaO and MgO, also a Na_2O precursor was tested), not previously tested. Direct firing at 1100 °C resulted in the desired wollastonite-diopside coupling. The strength-to-density was finally tuned by operating either on the topology of scaffolds or on the firing atmosphere (passing from air to N_2).

2. Experimental procedure

The initial reference of the research was the eutectic between wollastonite ($CaSiO_3$) and diopside ($CaMgSi_2O_6$), corresponding to the weight balance SiO_2:CaO:MgO=54:34.8:11.2 [17]. The silica fraction was supplied entirely by a preceramic polymer, consisting of a commercial silicone (Silres® H44, Wacker-Chemie GmbH, Munich, Germany), known to feature a ceramic yield in the air of ≈53 w% [15]). Calcium and magnesium oxide were given by salt precursors, particularly by calcium nitrate tetrahydrate ($Ca(NO_3)_2{\cdot}4H_2O$, Scharlab, Barcelona, Spain) and magnesium nitrate hexahydrate ($Mg(NO_3)_2{\cdot}6H_2O$, VWR International, Radnor, PA, USA). In analogy with previous experiments [7,15], the silicone-based mixture, to be used in stereolithography experiments, was modified by blending with a commercial photocurable resin (Standard Blend Transparent, FunToDo, Alkmaar, The Netherlands), in the proportions shown in Table 1.

The salts, unlike previous experiments, were not considered as solid fillers, but they were dispersed in form of emulsions, prepared in two steps. First, the H44 silicone resin, in powder form, was dissolved, by hand mixing, in a small amount of acrylic resin (5 g), and the mixture was left overnight under magnetic stirring, to ensure a complete homogeneity between the ingredients, forming a 'host' liquid phase. In a second step, a mixture was made by adding the calcium and magnesium nitrate salts to the rest of the acrylic resin (17 g), accompanied by 1g of Span 80 (Sorbitan Monooleate, TCI, Tokyo, Japan), acting as surfactant. The mixture was subjected firstly to magnetic stirring (for 30 min) and secondly to sonication (Bandelin Sonopuls HD 2070, Bandelin electronic GmbH & Co. KG, Berlin, Germany) until the salts were completely dispersed (15–20 min).

Table 1
Weight of the precursors that form the printing emulsions containing the dissolved salts.

Precursors	Ink composition [g]		
	S	SNa#1	SNa#2
Silres® H44	10.19	11.28	16.92
Calcium nitrate tetrahydrate	14.68	14.68	14.68
Magnesium nitrate hexahydrate	7.11	7.11	7.11
Sodium acetate trihydrate	0	1.23	1.84
FunToDo® resin	22	22	22
Span 80	1	1	1

The 'host' silicone-based liquid was finally mixed with the emulsion of salts in acrylic resin, by a second cycle of magnetic stirring (for 30 min) and sonication (10 min). In some formulations, sodium oxide was added, in the form of sodium acetate trihydrate ($CH_3COONa{\cdot}3H_2O$, AnalaR® NORMAPUR® ACS, VWR International, Radnor, PA, USA), to the salt emulsion, following the same procedure.

The mixtures were printed by means of a MSLA (masked stereolithography) equipment (Prusa SL1S, Prusa Research, Prague, Czech Republic), operating with visible light (λ=405 nm), from a LED array filtered by means of a monochrome LCD panel. Scaffolds with two different 3D lattice structures (DC and GM, both with nominal porosity of 85%, deriving from a preliminary computational study by the Rhinoceros® 6 program package, Robert McNeel & Associates, Seattle, WA, USA [7]), shown in Fig. 1, were manufactured using an exposure time of 10 s and layer thickness of 50 μm.

After printing, the components were removed from the printing platform and subsequently cleaned, by blowing compressed air and by immersion in isopropyl alcohol bath for 2 min. The cleaned structures underwent a final hardening step, again by exposition to high energy visible light (λ=405 nm), for 10 min, in a post-printing curing device (CW1S, Prusa Research, Prague, Czech Republic). Finally, the scaffolds were ceramized by a two-step heat treatment in static air or flowing nitrogen (0.5 °C/min up to 500 °C for 5 h, followed by heating at 2 °C/min up to 1100 °C for 1 h).

XRD analysis was performed using Bruker® X-ray diffractometer (D8 Advance, Karlsruhe, Germany) to identify the crystalline phases that formed during the heat treatment of the printed parts. The XRD analysis was carried out with a scanning 2θ range from 10° to 70° using a 0.05° and 2 s for each step. The identification of the different crystalline phases was determined using the Match! program package (Crystal Impact GbR, Bonn, Germany), supported by data from the PDF-2 database (ICDD-International Centre for Diffraction Data, Newtown Square, PA).

Density and porosity values were determined from geometrical measurements of regular blocks (geometrical density from the mass/volume ratio) and helium pycnometry (Micromeritics AccuPyc 1330, Norcross, GA), on whole scaffolds or on powdered materials, before and after heat treatment. Through the densities measurements, it was possible to compute open and total porosity of the scaffolds.

Morphological and microstructural characterizations were performed by optical stereomicroscopy (AxioCam ERc 5s Microscope Camera, Carl Zeiss Microscopy, Thornwood, New York, US) and scanning electron microscopy (FEI Quanta 200 ESEM, Eindhoven, The Netherlands). The compressive strength was measured using a universal materials testing machine (Quasar 25, Galdabini S.p.A., Cardano al

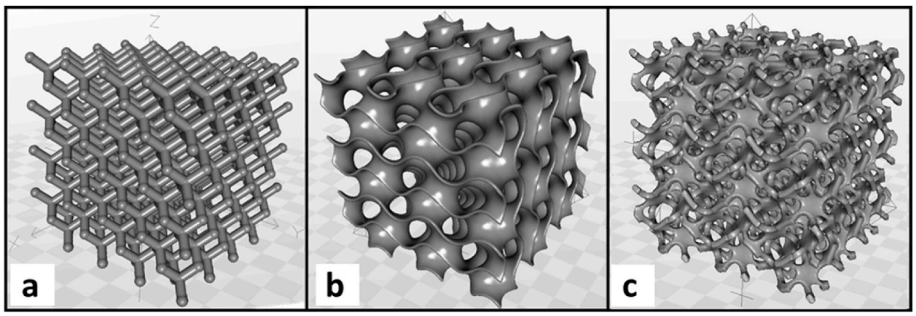

Fig. 1. Geometrical models for the manufacturing of highly porous scaffolds: a) diamond cubic (DC); b) gyroid; c) modified gyroid (GM).

Campo, Italy), operating at a crosshead speed of 0.5 mm/min; each data point represents an average value obtained by testing at least eight specimens.

3. Results and discussion

A first objective was the homogeneous dispersion of precursors, according to the adopted strategy. The heating produced by sonication was reputed as sufficient to determine the melting of hydrated Ca and Mg nitrates, in turn known for their low melting point (well below 100 °C).

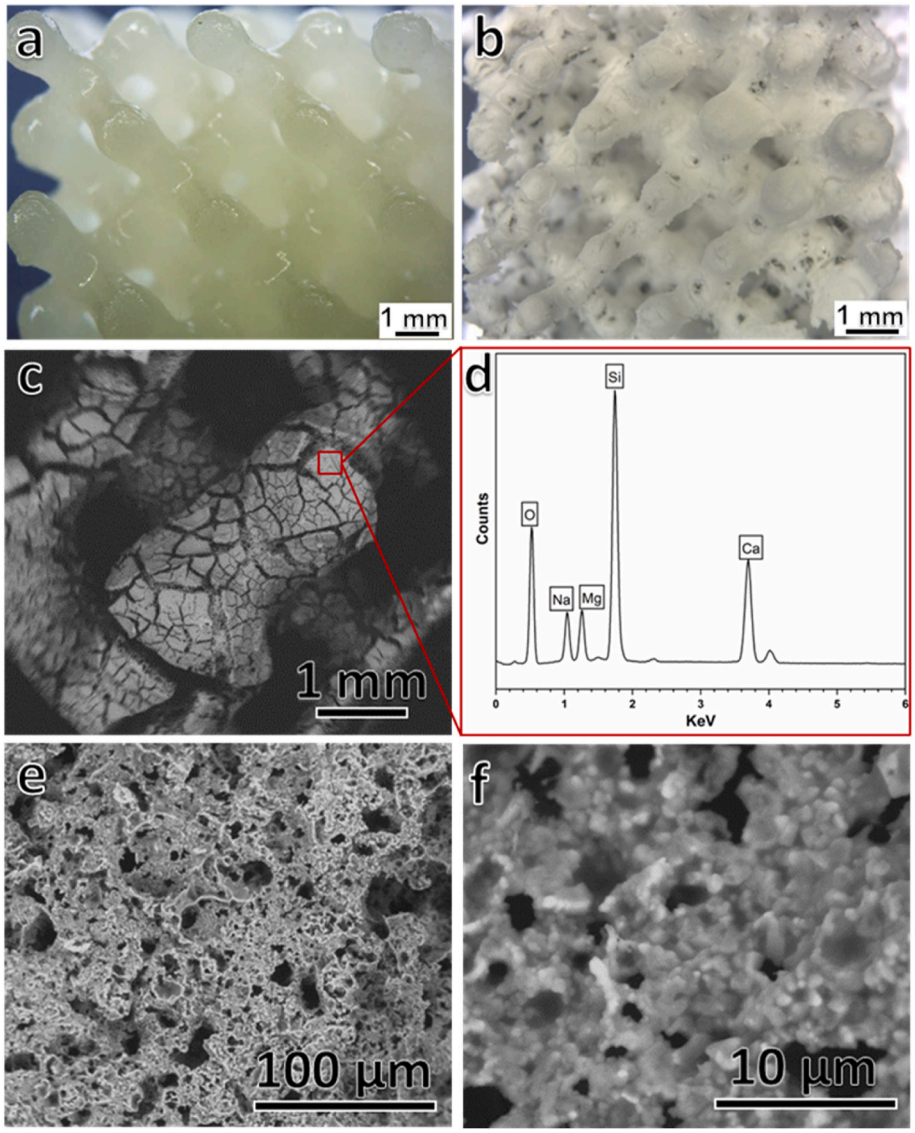

Fig. 2. Microstructural details of the printed scaffolds using the SNa2 emulsion: a,b) optical stereomicroscopy images of scaffold before (a) and after (b) ceramization in air; c) scanning electron microscopy image of struts after ceramization; d) EDS plot of the selected detail of the strut surface; e) detail of 'underneath' cellular structure; f) detail of the solid walls.

The addition of a surfactant was designed to promote the dispersion of liquid nano-sized droplets in acrylic resin, later turning in very fine nano-particles in the silicone-acrylic resin blend. Fig. 2a, obtained by high-resolution optical stereomicroscopy, provides a simple confirmation of the expected behavior: all printed scaffolds were nearly transparent and highly homogeneous, i.e. they did not exhibit any gradient or sign of agglomeration of suspended particles.

The first firing experiments (up to 1100 °C), on scaffolds with DC geometry, printed from the reference formulation (S), were unsuccessful. The fired samples, although preserving the scaffold geometry, were so severely cracked that they collapsed into powder just by gentle pressure and is the reason why they are not shown in the figures.

S formulation was not satisfying also in terms of phase evolution, as demonstrated by Fig. 3 (bottom pattern). Diopside crystals ($CaMgSi_2O_6$, PDF#78–1390), clearly formed, but not accompanied by wollastonite. The diffraction peaks, which could not be attributed to diopside, actually matched with those of di-calcium silicate (Ca_2SiO_4, PDF#31–0302) and crystalline silica (quartz, PDF#74–1496). In other words, for the part not involved in diopside, CaO did not react in 1:1 M proportion with SiO_2 (yielding wollastonite). Some local fluctuations in the distribution of calcium oxide precursor evidently favored the formation of crystals with a higher CaO/SiO_2 ratio, on one hand, leaving some unreacted silica (quite surprisingly crystallized in form of quartz, α polymorph, PDF#74–1496), on the other.

In analogy with previous research on wollastonite-diopside polymer-derived ceramics [11,13,18], the S formulation was corrected in order to develop some extra liquid phase, upon firing. In line with that, sodium was added to the base formulation, giving rise to samples SNa#1 and SNa#2. The extra phase was expected to have a multiform impact. First, as previously mentioned, the liquid was intended to catalyse the ionic interdiffusion; second, the liquid phase could provide some sealing of the cracks, developed as a result of internal stresses, in turn due to gas release in the solid determined by the ceramic transformation of the silicone, creating a scaffold with improved mechanical properties [18]. The Na_2O addition was balanced by an increase of silicone (and obviously of silicone-derived SiO_2), with the perspective of forming a sodium silicate liquid phase, upon heat treatment, possibly transforming into glass phase upon cooling. As written above, although not formed by crystallization of a homogeneous parent glass, Na-containing blends were designed to yield 'polymer-derived glass-ceramics'.

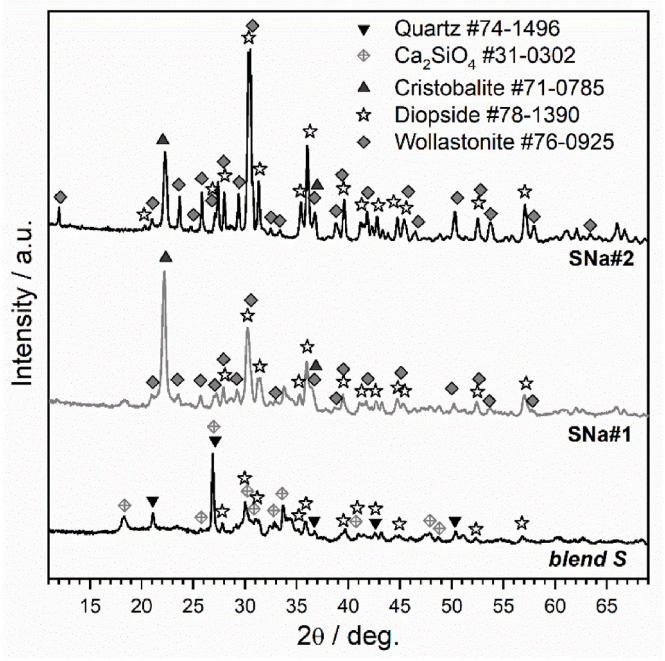

Fig. 3. X-ray diffraction patterns of printed scaffolds, made from various compositions, after firing at 1100 °C for 1 h.

The progressive addition of sodium oxide (and extra silica) effectively led to the simultaneous crystallization of wollastonite ($CaSiO_3$, PDF#76–0925) and diopside ($CaMgSi_2O_6$, PDF#78–1390). As shown by Fig. 3, the intensity of the diffraction peaks attributed to these phases increased substantially passing from SNa#1 to SNa#2; in parallel, crystalline silica, appearing as cristobalite (low temperature, α polymorph, PDF#71–0785), decreased. The overall oxide composition, from SNa#2 composition, actually resembles that of wollastonite-diopside glass-ceramics with proven bioactivity and biocompatibility [18].

Printed scaffolds from SNa#2 led to ceramic parts which preserved both original geometry (Fig. 2b) and sufficient structural integrity to be possibly handled, compared to printed scaffolds from S formulations. The sealing of cracks, however, was not confirmed; as shown by Fig. 2c, cracks were likely limited but not eliminated. Energy dispersive X-ray spectroscopy (EDS) analysis of the top surface (Fig. 2d) actually shows an enrichment of Na: some sodium silicate phase evidently formed, as expected, but it 'sealed' the surface before the evolution of gas, from multiple reactions (associated with the decomposition of the Ca and Mg nitrate precursors and transformation of silicone into ceramic), could be completed. It is worth noting that cracks reveal a quite interesting underneath 'spongy' structure (Fig. 2e), with the solid phase evidencing a multitude of tiny crystals (Fig. 2f). The combination of macro-porosity from printing, with micro-porosity from the particular gas evolution, is reputed as highly favorable in the perspective of bone tissue engineering, since it would facilitate cell attachment and proliferation, and help the transport of nutrients [22].

The extent of the cracking could be probably reduced, by adopting an updated firing schedule. For the sake of simplicity, leaving the heat treatment unchanged, some changes were explored just in the topology of printed scaffolds. Fig. 1b clearly shows that passing from a diamond cell lattice (DC) to a gyroid, with the same nominal porosity, implies the replacement of relatively thick 'beam' struts with thinner walls, separating helicoidal channels. From a polymer-derived system, thinner membranes could facilitate the gas evolution. The modified gyroid-like structure (GM, see Fig. 1c) was adopted as a compromise: it kept, from gyroid, relatively thin walls, whereas holes in the same wall favored the pore interconnectivity, typical of diamond cell. As shown by Fig. 4a, the cracking was effectively reduced with GM scaffold geometry; progressive magnifications (Fig. 4b and c) confirm the presence of dense surface 'islands', cladding a 'spongy' underneath structure.

The scaffolds were compared in terms of correlation between strength and porosity. For cellular materials, with completely open porosity, the compressive strength (σ_c) may be predicted from the bending strength of the solid phase ($\sigma_{bend,SP}$), according to the Gibson-Ashby model [23]:

$$\sigma_c = C \cdot \sigma_{bend,SP} \cdot \rho_{rel}^{3/2}$$

where C is a dimensionless constant (≈0.2) and ρ_{rel} is defined as the relative density (ρ_{rel}=(1-P)/100, where P is the total porosity).

Knowing the compressive strength and total porosity value of a cellular solid, the equation can be reversed and provide an 'apparent' bending strength of the solid phase. The value is 'apparent' since the model assumes open-celled bodies as lattices with structural elements represented by straight and thin beams, welded together, undergoing bending. Operating with scaffolds of quite complicated structure, as in the present case, the calculated value of $\sigma_{bend,SP}$ may be considered as a measure of integrity: large deviations from the real bending strength of the solid may suggest the presence of cracks or internal stresses, favoring mechanical failure [7].

As reported in Table 2, the fired DC scaffolds had a completely open porosity of ~90 vol%. Such value cannot be seen as a direct effect of the printing; starting from the model, with 85% porosity, the as-printed scaffold, according to limitations in the resolution of the equipment,

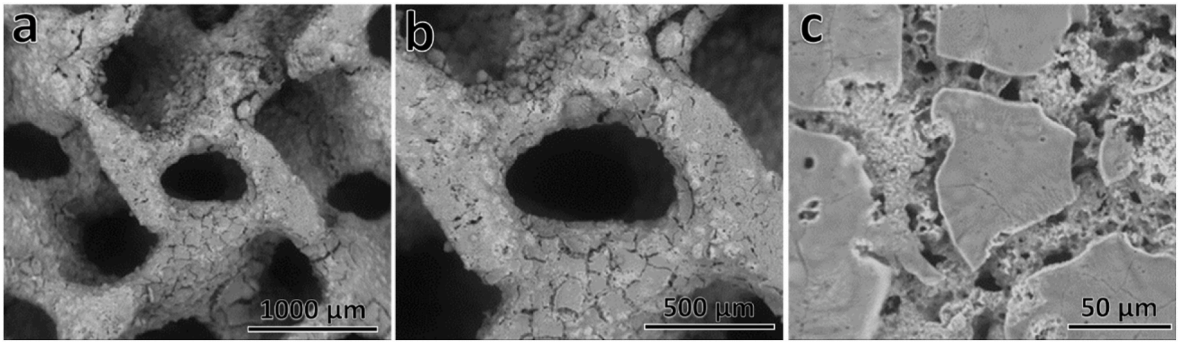

Fig. 4. Microstructural details of GM scaffold, printed using the SNa#2 emulsion, after firing.

Table 2
Summary of physical properties of heat-treated SNa#2 scaffolds.

Design	Atm	ρ_{geom} [g/cm^3]	ρ_{app} [g/cm^3]	ρ_{true} [g/cm^3]	P_{open} [%]	P_{tot} [%]	σ_c [MPa]	Apparent $\sigma_{bend,SP}$ [MPa]
DC	Air	0.26 ± 0.05	2.68 ± 0.06	2.83 ± 0.07	90 ± 1.9	91 ± 1.8	0.3 ± 0.1	55.6
GM	Air	0.45 ± 0.03	2.86 ± 0.11	2.83 ± 0.04	84 ± 1.1	84 ± 1.0	1.3 ± 0.2	103.2
DC	N_2	0.72 ± 0.16	2.37 ± 0.05	2.42 ± 0.06	70 ± 1.5	70 ± 1.8	4.2 ± 0.7	127.8
GM	N_2	1.07 ± 0.16	2.39 ± 0.03	2.42 ± 0.05	55 ± 1.5	56 ± 1.8	11.7 ± 1.7	n.d.

featured a porosity of ~75 vol%. Additional porosity was achieved according to the above-discussed gas evolution. With the observed relative density (~0.1), despite the very low compressive strength (σ_c) of 0.3 MPa, DC scaffolds are interesting. In fact, the 'apparent' bending strength of the solid phase exceeded 50 MPa, not far from the bending strength of pore-free soda-lime glass (~70 MPa) [24]. The high strength claimed for silicates (particularly Ca–Mg silicates) [25,26] evidently provided some compensation of the weakening effect of extensive cracking.

GM scaffolds could not be directly compared to DC scaffolds, due to the different porosity; the nearly double value of $\sigma_{bend,SP}$ is consistent with the limitation of cracks. The strength-to-density ratio (~2.9 MPa cm^3/g) is also in quite good agreement with that of polymer-derived wollastonite-diopside foams (2.5–5 MPa cm^3/g) [11,13].

A further tuning possibility relies, operating with silicone polymers, on the modification of the silicone-to-ceramic transformation, by performing it in N_2 atmosphere instead of air [27,28]. In particular, H44 is known to yield, when fired in not-oxidative atmosphere, an oxycarbide ceramic residue with the nominal stoichiometry of $Si_3O_{4.6}C_{8.45}$ [7], which could be seen as a combination of silica (SiO_2), silicon carbide (SiC) and carbon (C), as follows:

$$Si_3O_{4.6}C_{8.45} \longleftrightarrow 2.3\ SiO_2 + 0.7\ SiC + 7.75\ C$$

Some systems have been studied in the hypothesis of interaction between oxide fillers and the silica fraction of the oxycarbide residue, with the rest remaining as extra, C-containing inert phases [28,29]. The exact reaction mechanism, however, is still unclear and may be sensitive to the particular processing conditions. In particular, for recent silicate bioceramics (developed by stereolithography of silicone-acrylate resin blends) [7], it has been found that H44 actually yields, in nitrogen, just silica and pyrolytic carbon, with the overall SiO_2 amount comparable to that achieved by firing in air. Such observation motivated the firing of DC and GM scaffolds, in N_2, without any change in the proportions between constituents.

As illustrated by Fig. 5, the firing in nitrogen led to much less crystallized samples. The diffraction peaks are still consistent with both wollastonite ($CaSiO_3$, PDF#76–0925) and diopside ($CaMgSi_2O_6$, PDF#78–1390), but the limited intensity suggests a reduced crystallization degree. Interestingly, no cristobalite trace could be detected.

The change in firing atmosphere favored the integrity of samples, in good agreement with previous findings [29]. In particular, it is known

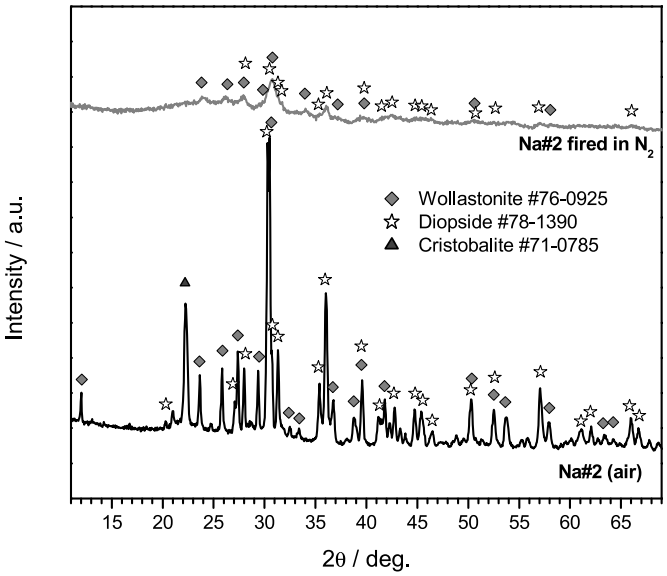

Fig. 5. Comparison of phase evolution by firing, in air and nitrogen, of scaffolds based on SNa#2 blend.

that the decomposition of the Si–R bonds, for silicones subjected to thermo-oxidative process is extremely exothermic [30]; firing in N_2 determines an alternative, complex path. The embedding of pyrolytic carbon, in non-oxidative atmosphere, obviously corresponds to a sensible reduction of gas generation. We cannot also exclude a positive contribution of avoided crystallization of cristobalite, well-known to induce micro-cracking, due to sensible volumetric changes in the transformation from high temperature (β) form to low temperature variant (α).

The reduced gas generation is consistent with the development of much denser structures (see Table 2): as shown by Fig. 6, the fired materials (Fig. 6b), except for a substantial shrinkage (of ~70% volumetric shrinkage), kept a quite strict similarity to the as printed bodies (Fig. 6a). In other words, if the printing caused some coarsening of printed bodies, compared to the geometrical model (owing to the above-mentioned low resolution of the same printer), the firing could 'freeze'

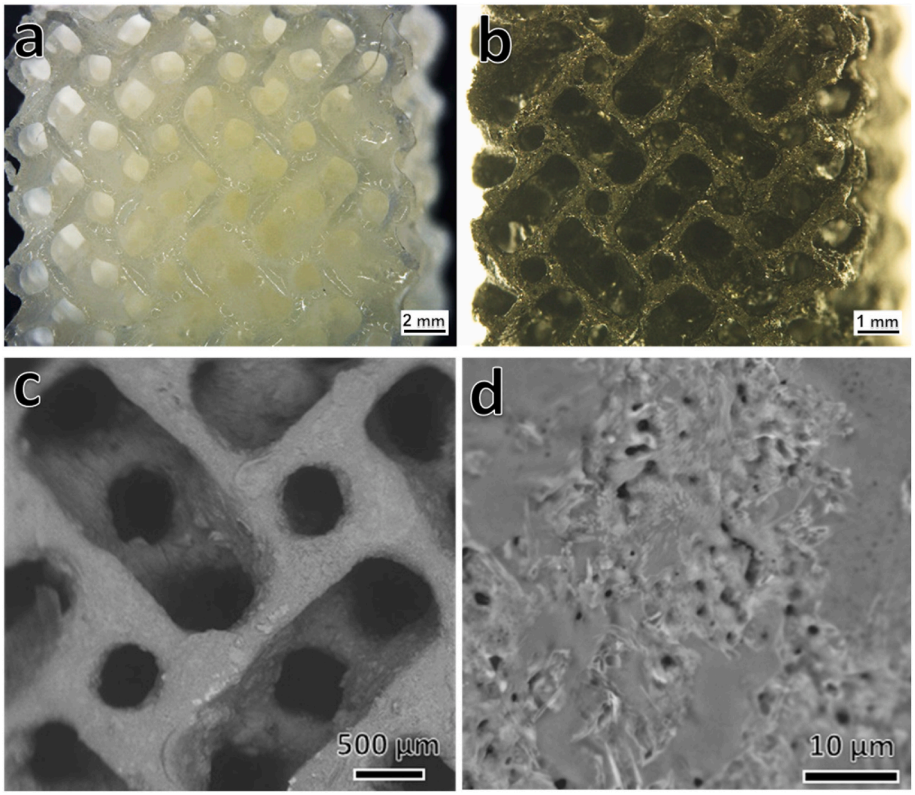

Fig. 6. Microstructural details of modified gyroid (GM) of scaffolds from SNa#2 blend, fired in N_2: a,b) optical images of printed sample before (a) and after (b) firing; c,d) high magnification SEM images.

the structure, with much less extra porosity developed in the ceramic conversion. The absence of cracks and the formation of crystals is illustrated by scanning electron microscopy images (Fig. 6c and d, respectively).

The superior integrity obviously affected the mechanical properties. GM scaffolds achieved a compressive strength well exceeding 10 MPa, but the relatively low porosity impedes any comparison, with other scaffolds, on the basis of the Gibson-Ashby model (applicable for porosity exceeding 70%); for DM scaffolds, on the contrary, the application of the Gibson-Ashby gives a $\sigma_{bend,SP}$ value above 120 MPa (with a strength-to-density exceeding 6.5 MPa cm^3/g).

In conclusion, the present investigation confirms the potential of preceramic polymers in the additive manufacturing of bioceramics, with significant elements of novelty; the adopted strategy of homogenization of CaO and MgO precursors, especially for the firing in nitrogen, may pave the way even to completely amorphous materials ('polymer-derived bioglasses'), simply by revision of the processing temperatures and balance between main oxides. The chemical modification of the ceramic residue of silicones is achieved in conditions of impressive simplicity, unlike attempts relying on metallorganic compounds [31] which, in addition, did not comprise the integration with additive manufacturing, here shown. Future efforts will be undoubtedly needed for the improvement of cellular structures, by application of the developed blends in more advanced stereolithography printers, and for the effective assessment of biocompatibility, bioactivity and bioresorbability, by a series of cell culture tests.

A further potential, to be carefully discussed, concerns the inclusion of pyrolytic carbon, visible from the black color of scaffolds fired in N_2 (see Fig. 6b). Carbon polymorphs are becoming more and more promising for enhancing osteogenic differentiation and providing extra functionalities to biomaterials [32]; as an example, the excellent absorption capability in the near infrared (NIR) range of C-containing biomaterials encourages photothermal heating [28], for disinfection as well as for therapy of tumors [16,33–35].

4. Conclusions

A commercial silicone polymer is confirmed in its great potential for the stereolithography of ceramic components with complex geometry. It provides a double advantage, i.e. it may be easily blended with commercial acrylate resin and it leads to biocompatible and bioactive Ca and Ca–Mg silicates, by interaction with oxide (CaO, MgO and Na_2O) inclusions. The latter are shown to be feasible, for the first time, from emulsions. The feasibility of emulsions involving multiple oxide precursors offers many opportunities, here only partially explored, upon ceramic transformation, based on quantity of gas released, quantity of transient liquid formed, degrees of densification and crystallization, fidelity to the geometry of starting models etc. The approach is so flexible that it does not enable easy modifications on formulations, but also on geometrical modelling and on firing atmosphere. Firing in nitrogen, in particular, emerges as a solution for the development of a new generation of glass-ceramics, not relying on the preparation of any parent glass.

Declaration of competing interest

The authors declare that they have no known competing financial interests or personal relationships that could have appeared to influence the work reported in this paper.

Acknowledgements

The authors thank Mr Paolo Reginato and Ms Laura Degli Agostini (MSc students, University of Padova), for experimental assistance. FMS acknowledges the External Scholarship granted by the Scientific and Technical National Research Council (CONICET), Argentina.

References

[1] G. Rasiya, A. Shukla, K. Saran, Additive manufacturing-A review, Mater. Today: Proc. 47 (2021) 6896–6901.

[2] C. Zhang, F. Chen, Z. Huang, M. Jia, G. Chen, Y. Ye, Y. Lin, W. Liu, B. Chen, Q. Shen, L. Zhang, E.J. Lavernia, Additive manufacturing of functionally graded materials: a review, Mater. Sci. Eng. 764 (2019), 138209.

[3] A.L.R. Prathyusha, G.R. Babu, A review on additive manufacturing and topology optimization process for weight reduction studies in various industrial applications, Mater. Today: Proc. 62 (2022) 109–117.

[4] X. Wang, S. Xu, S. Zhou, W. Xu, M. Leary, P. Choong, M. Qian, M. Brandt, Y.M. Xie, Topological design and additive manufacturing of porous metals for bone scaffolds and orthopaedic implants: a review, Biomaterials 83 (2016) 127–141.

[5] J. Hu, J.H. Wang, R. Wang, R.X.B. Yu, Y. Liu, D.A. Baur, Analysis of biomechanical behavior of 3D printed mandibular graft with porous scaffold structure designed by topological optimization, 3D Print Med 5 (2019) 5.

[6] C. Qian, K. Hu, J. Li, P. Li, Z. Lu, The effect of light scattering in stereolithography ceramic manufacturing, J. Eur. Ceram. Soc. 41 (2021) 7141–7154.

[7] P. Ożóg, H. Elsayed, L. Grigolato, G. Savio, J. Kraxner, D. Galusek, E. Bernardo, Engineering of silicone-based blends for the masked stereolithography of biosilicate/carbon composite scaffolds, J. Eur. Ceram. Soc. 42 (2022) 6192–6198.

[8] J. Schmidt, P. Colombo, Digital light processing of ceramic components from polysiloxanes, J. Eur. Ceram. Soc. 38 (2018) 57–66.

[9] P. Colombo, G. Mera, R. Riedel, G.D. Sorarù, Polymer-Derived-Ceramics: 40 years of research and innovation in advanced ceramics, J. Am. Ceram. Soc. 93 (2010) 1805–1837.

[10] E. Zanchetta, M. Cattaldo, G. Franchin, M. Schwentenwein, J. Homa, G. Brusatin, P. Colombo, Stereolithography of SiOC ceramic microcomponents, Adv. Mater. 28 (2016) 370–376.

[11] A. Dasan, H. Elsayed, J. Kraxner, D. Galusek, P. Colombo, E. Bernardo, Engineering of silicone-based mixtures for the digital light processing of Åkermanite scaffolds, J. Eur. Ceram. Soc. 40 (2020) 2566–2572.

[12] L. Fiocco, H. Elsayed, L. Ferroni, C. Gardin, B. Zavan, E. Bernardo, Bioactive wollastonite-diopside foams from preceramic polymers and reactive oxide fillers, Materials 8 (2015) 2480–2494.

[13] H. Elsayed, A. Zocca, G. Franchin, E. Bernardo, P. Colombo, Hardystonite bioceramics from preceramic polymers, J. Eur. Ceram. Soc. 36 (2016) 829–835.

[14] L. Fiocco, S. Li, M.M. Stevens, E. Bernardo, J.R. Jones, Biocompatibility and bioactivity of porous polymer-derived Ca-Mg silicate ceramics, Acta Biomater. 50 (2017) 56–67.

[15] H. Elsayed, P. Rebesan, M.C. Crovace, E.D. Zanotto, E. Bernardo, Biosilicate® scaffolds produced by 3D-printing and direct foaming using preceramic polymers, J. Am. Ceram. Soc. 102 (2018) 1010–1020.

[16] S. Fu, H. Hu, J. Chen, Y. Zhu, S. Zhao, Silicone resin derived larnite/C scaffolds via 3D printing for potential tumor therapy and bone regeneration, Chem. Eng. J. 382 (2020), 122928.

[17] M.A. Sainz, P. Pena, S. Serena, A. Caballero, Influence of design on bioactivity of novel $CaSiO_3$–$CaMg(SiO_3)_2$ bioceramics: in vitro simulated body fluid test and thermodynamic simulation, Acta Biomater. 6 (2010) 2797.

[18] L. Fiocco, H. Elsayed, J.K.M.F. Daguano, V.O. Soares, E. Bernardo, Silicone resins mixed with active oxide fillers and Ca–Mg Silicate glass as alternative/integrative precursors for wollastonite–diopside glass-ceramic foams, J. Non-Cry. Solids. 416 (2015) 44–49.

[19] M. Porras, C. Solans, C. González, J.M. Gutiérrez, Properties of water-in-oil (W/O) nano-emulsions prepared by a low-energy emulsification method, Colloids Surf. A Physicochem. Eng. Asp. 324 (2008) 181–188.

[20] A. Gupta, H.B. Eral, T.A. Hatton, P.S. Doyle, Nanoemulsions: formation, properties and applications, Soft Matter 12 (2016) 2826–2841.

[21] F.M. Stabile, A. Famengo, D. Pedron, H. Elsayed, E. Bernardo, Functional carbon-based bioglass nanocomposite scaffolds from vat photopolymerization of a novel preceramic polymer-based nanoemulsion, Addit. Manuf. (2023), 103731.

[22] Y. Liu, S. Yang, L. Cao, X. Zhang, J. Wang, C. Liu, Facilitated vascularization and enhanced bone regeneration by manipulation hierarchical pore structure of scaffolds, Mater. Sci. Eng. C 110 (2020), 110622.

[23] L.J. Gibson, M.F. Ashby, Cellular Solids: Structure and Properties, Cambridge university Press, Cambridge, UK, 1999.

[24] A.S. Llaudis, M.J.O. Tari, F.J.G. Ten, E. Bernardo, P. Colombo, Foaming of flat glass cullet using Si_3N_4 and MnO_2 powders, Ceram. Int. 35 (2009) 1953–1959.

[25] C. Wu, Methods of improving mechanical and biomedical properties of Ca–Si-based ceramics and scaffolds, Expet Rev. Med. Dev. 6 (2009) 237–241.

[26] C. Wu, J. Chang, A review of bioactive silicate ceramics, Biomed. Mater. 8 (2013), 032001.

[27] M. Scheffler, T. Takahashi, J. Kaschta, H. Muensted, P. Buhler, P. Greil, Pyrolytic decomposition of preceramic organo polysiloxanes, Ceram. Trans. 115 (2000) 239–250.

[28] F. Dogrul, P. Ożóg, M. Michálek, H. Elsayed, D. Galusek, L. Liverani, A. R. Boccaccini, E. Bernardo, Polymer-derived biosilicate®-like glass-ceramics: engineering of formulations and additive manufacturing of three-dimensional scaffolds, Materials 14 (2021) 5170.

[29] F. Dogrul, S. Bortolin, D. Del Col, N. Dengo, D. Pedron, M. Michalek, H. Elsayed, D. Galusek, E. Bernardo, Polymer-derived Biosilicate-C composite foams: phase development and photothermal effect, J. Eur. Ceram. Soc. 41 (2021) 380–388.

[30] D. Yang, W. Zhang, B. Jiang, Ceramization and oxidation behaviors of silicone rubber ablative composite under oxyacetylene flame, Ceram. Int. 39 (2013) 1575–1581.

[31] I. Gonzalo-Juan, R. Detsch, S. Mathur, E. Ionescu, A.R. Boccaccini, R. Riedel, Synthesis and in vitro activity assessment of novel silicon oxycarbide-based bioactive glasses, Materials 9 (2016) 959.

[32] D. Shao, M. Lu, D. Xu, X. Zheng, Y. Pan, Y. Song, J. Xu, M. Li, M. Zhang, J. Li, G. Chi, L. Chen, B. Yang, Carbon dots for tracking and promoting the osteogenic differentiation of mesenchymal stem cells, Biomater. Sci. 5 (2017) 1820–1827.

[33] M. Zheng, Y. Li, S. Liu, W. Wang, Z. Xie, X. Jing, One-pot to synthesize multifunctional carbon dots for near infrared fluorescence imaging and photothermal cancer therapy, ACS Appl. Mater. Interfaces 8 (2016) 23533–23541.

[34] J. Yu, L. Yang, J. Yan, W.C. Wang, Y.-C. Chen, H.-H. Chen, C.-H. Lin, Carbon Nanomaterials for Photothermal Therapies Carbon Nanomaterials for Bioimaging, Bioanalysis, and Therapy, John Wiley & Sons Ltd, 2018, pp. 309–340.

[35] J. Xu, K. Yao, Z. Xu, Nanomaterials with a photothermal effect for antibacterial activities: an overview, Nanoscale 11 (2019) 8680–8691.